OPTIMIZATION OF HEAT EXCHANGER MANIFOLD

Marcela G. Hinojosa Almaraz **Abdulwahab Sayes** **LloydAnthony Blackwood** **Boris Lokossou**

ABSTRACT

The global transition toward cleaner energy systems requires technologies that reduce building energy demand and improve the efficiency of heating and cooling infrastructure. MicroEra Power's THERMAplus system addresses this need through thermal energy storage, but its manifold heat exchanger can experience nonuniform flow and pressure losses that increase pumping power. This project aimed to optimize the manifold orifice configuration while maintaining the existing panel geometry. Four half-scale manifold assemblies were developed and evaluated: baseline-baseline, optimized-baseline, optimized-optimized, and optimized-open. Computational fluid dynamics were used before manufacturing to compare pressure drop and flow uniformity, while physical testing measured pressure drop, flow output, leakage, and thermal distribution across the panels. The optimized designs all reduced pressure drop by more than 5% relative to the baseline, with the optimized-baseline configuration producing the largest pumping power reduction of 40.47%. However, because the operating system may reverse flow direction, the optimized-optimized configuration was recommended as the most practical final design. The results show that targeted changes to orifice spacing can improve manifold performance, reduce pumping energy, and support the broader implementation of efficient thermal energy storage systems.

PROBLEM DEFINITION

MicroEra's heat exchanger system utilizes a manifold with orifices along its length, through which a water-glycol mixture is forced to aid the energy transfer process for building heating or cooling (Appendix D, Figure D5). Currently, as fluid travels through the manifold, it experiences pressure losses that force the pump to work harder and draw more electricity to maintain adequate flow. The goal of this project is to optimize flow through the manifold to maintain or increase heat transfer, which will reduce carbon emissions by requiring less electricity to achieve the same performance. Optimizing MicroEra's manifold system will increase product energy efficiency and reduce the electricity consumption of the buildings in which they are installed; this, in turn, will lower carbon emissions and help slow the progress of climate change.

REQUIREMENTS, SPECIFICATIONS, DELIVERABLES

For this Project, the deliverables are a prototype device of the solution to the problem; a technical report including the process for solution, simulations, and test data; and the CAD model of the optimized panels. The requirements of this project include lowering pumping power by decreasing pressure drop across the system while maintaining heat transfer through flow uniformity, leaving the general geometry and dimensions of the manifold and panels untouched, and only modifying the geometry and configuration of the orifices. To achieve those requirements, the specifications dictate a minimum of 5% improvement in system efficiency through improving the flow and having an optimized system with a 3 years return on investment.

CONCEPTS

Table 1 shows the designs agreed upon for manufacturing and testing in a Pugh matrix.

Concepts Name	Baseline (B1 – B1)	Concept 1 (C1 – B1)	Concept 2 (C1 – C1)	Concept 3 (C1 – Open)
Ease of Manufacture	0	0	0	0
Pressure Drop	0	-	+	+
Time of Manufacture	0	0	0	-
Flow Uniformity	0	+	+	+
Total	0	0	+2	+1

These design concepts were developed based on sponsor requirements, flow calculations, simulations, and previous iterations. The primary intention was to "choke" the flow at the bottom of the manifold to force fluid through the upper orifices. An initial pipe flow test (Appendix D, Figure D1) confirmed that the bottom orifices produced significantly faster jets compared to the higher orifices. To balance performance with manufacturing ease, the final design was limited to three tool

 Copyright © 2026 by ASME

changes for orifice adjustments; consequently, the manifold was divided into three sections: Zones A, B, and C.

The first iteration of the MATLAB fluid calculator (Appendix E, Code E1) produced velocity and pressure profiles (Appendix D, Figure D3) showing a non-linear increase in both variables as flow travels down the manifold. This suggests that gravity is more dominant than frictional losses. While this first version of the code did not fully conserve mass flow, it was used to analyze the trend of the curve—rather than as a source of hard numerical facts—to determine how to reduce flow at the bottom. After multiple iterations, the results (Appendix D, Figure D4) showed that choking the bottom flow to direct it toward the top successfully increases flow uniformity and implies a decreased pressure drop. These findings led to a refined inlet manifold design called "C1." Computational Fluid Dynamics (CFD) was then used to refine C1 and create additional concepts with configurations optimized for manufacturing.

For testing purposes, all concepts explained below are the 50% scale of the original system. To achieve even flow through the panels, the goal was to ensure each zone collected a similar volume of fluid.

The concepts are as follows:

- Baseline (B1-B1): 'B1' serves as the baseline outlet manifold with 20 mm spacing resulting in 27 orifices. This manifold was made as a scaled model to reflect the actual full-sized models.
- Concept 1 (C1–B1): Features inlet manifold 'C1' with orifice configurations as such: Zone C (7 holes, 25 mm spacing), Zone B (9 holes, 20 mm spacing), and Zone A (11 holes, 15 mm spacing).
- Concept 2 (C1–C1): Replaces the baseline outlet manifold with the 'C1' configuration.
- Concept 3 (C1–Open): Utilizes the 'C1' inlet with an 'Open' outlet manifold containing 39 equally spaced orifices.

MECHANICAL ANALYSIS

Tolerance Analysis

For proper operations, the orifices along the PVC/manifold pipe must be centered within a 6.35 mm (0.25 inches) wide channel to ensure fluid flows directly into the channel without interference or blockage. Therefore, it is necessary to perform a tolerance analysis on the orifice placements along the pipe's vertical axis. The critical dimension is the total lateral deviation from the centerline, because the allowable deviation must ensure the edge of the orifice does not exceed the channel width. Using a worst-case analysis, the "gap" must be positive as shown in Equation 1:

$$\frac{CW}{2} - \left(PT_{v-block} + \frac{D_{max}}{2}\right) \geq 0 \quad (1)$$

With a channel width (CW) of 6.35 mm, the max orifice diameter (D_{max}) of 3.175 mm (0.125 inches), and a V-block positional tolerance (PT) of 0.002 mm, a clearance value of 1.5855 mm (0.0624 inches) is achieved.

Fatigue Analysis

The component of the system most vulnerable to fatigue is the Polyvinyl chloride (PVC) manifold. These manifolds are constructed from 31.75 mm (1-¼ inch) Schedule 40 PVC Pipes with a wall thickness of 3.91 mm (0.154 inches). For proper operation, the pipes must be able to withstand the internal pressure of the fluid passing through during its high cycle rate. Plastics exhibit different behaviors than metals do, and their strengths can vary based on operating temperature as well. So, to ensure fatigue failure will not occur, a conservative approach was taken.

While the standard rule of thumb for metals is to set the endurance limit (Se') to 50% of the ultimate strength according to Shigley's Mechanical Engineering Design, we used a more conservative limit for this material as shown in Equation 7 and have our fatigue limit at 1.65 MPa [6].

$$S_e' = 0.2 \cdot S_{burst} \quad (7)$$

During operation, the peak pressure of 8.5 kPa was measured at the top. Assuming pressure increases due to hydrostatic head, the lowest orifice at the bottom of the pipe would experience an increase of 14.48 kPa. Then applying a 5x safety multiplier because of start-up pressure spikes leads to a peak pressure of 72.4 kPa.

Inside the pipe, the max localized stress would be located near the orifice. Using 72.4 kPa as our operating pressure gives a nominal hoop stress of 0.39 MPa. Then applying a theoretical stress concentration factor of 3, assuming the offices are cleaned and deburred results in a maximum localized stress of 1.17 MPa. With all the conservative approaches taken, this max localized stress is only 71% of our endurance limit implying a negligible risk of fatigue failure and confirming that the system is overdesigned for our specified operating conditions.

Fastener Torque Calculation

The pipe fittings at the system's inlet and outlet are vital components. Sealing rings were 3D-printed, tapped, and glued to hold the pipe fittings that connect to standard garden hoses. To prevent leakage, the fitting fastener must provide a clamping force exceeding the separation force created by the internal fluid. Using a conservative approach with the previously specified peak pressure of 72.4 kPa and a standard 19.05 mm (¾ inch) diameter fitting, we establish a pre-load of 20.64 N (4.640 lb_f). Using Equation 8 and assuming a torque factor (K) of 0.20, the required torque is 0.0786 Nm (0.058 ft-lb) [7]. Hand-tightening the garden hose onto the models provides a torque significantly higher than this requirement.

$$T = K \cdot F_i \cdot d \quad (8)$$

Copyright © 2026 by ASME

Material Selection

When deciding which material to use to build the models, three options were evaluated: PVC, Polypropylene, and acrylic tubing. Acrylic tubing was eliminated when the focus of testing shifted from visual flow observation toward thermal camera analysis. In terms of physical properties, PVC and Polypropylene are very similar. PVC possesses a tensile strength of 34–62 MPa (4,930–8,990 psi), while Polypropylene ranges from 25–40 MPa (3,625–5,800 psi). Both materials maintain comparable operating temperatures, with Polypropylene at 82.2 °C (180 °F) and PVC at 60-95 °C (140-203 °F) [8]. PVC was selected because it being more accessible. It reduced manufacturing time needed to deburr as the orifices drilled on the PVC produced clean edges.

Fundamental Mechanical Analysis

The analysis of the pressure drops and flow rate across the manifold at each individual orifice utilized the parallel flow assumptions of:

$$Q_{in} = \sum Q_{out} \quad (2)$$

$$h_{L,1} = h_{L,2} = h_{L,3} \quad (3)$$

Where Q is volumetric flow rate and h_L is major head loss. The first equation summarizes that the volumetric flow rate going into the system must flow out, and all head losses through each orifice must be equal.

The Mechanical Energy Equation was used at each junction to calculate the pressure drop as depth in the manifold decreased.

$$\frac{P_1}{\gamma} + \frac{v_1^2}{2g} + h_1 = \frac{P_2}{\gamma} + \frac{v_2^2}{2g} + h_2 + h_{major} + h_{minor} \quad (4)$$

To capture the losses of the fluid as the water descends through the manifold and flows through orifices, the Dary-Weisbach equation and minor head loss formulas were implemented.

$$Darcy - Weisbach: h_{major} = f\frac{L}{D}\frac{v^2}{2g} \quad (5)$$

$$Minor\ Head\ Loss: h_{minor} = K\frac{v^2}{2g} \quad (6)$$

Where f is the Darcy friction factor, L is the distance the fluid traveled between orifices, D is the diameter of the manifold, K is the minor loss coefficient, and g acceleration due to gravity. This analysis aligns more closely with the second version of the MATLAB script, which conserves mass flow, but operates with the limitation of a five-orifice maximum.

Computer-Based Analysis

Computational fluid dynamics, CFD, was used as a preliminary design and comparison tool before manufacturing the physical manifold prototypes. The main purpose of the CFD analysis was to confirm whether the design assumptions were reasonable, provide idealized results for later comparison with physical testing, and support iterative optimization of the manifold concepts. Since the project's goal was to improve flow uniformity across the panel while reducing pressure drop, CFD was used to visualize pressure and velocity distributions inside each manifold assembly before committing to manufacturing. This approach allowed the team to evaluate the different concepts (B1-B1, C1-B1, C1-C1, C1-Open) under the same boundary conditions.

The simulations were performed using the CFD Designer function in Siemens NX. Each model was set up as an internal flow simulation with water as the working fluid. Gravity was included in the negative z-direction to represent the vertical orientation of the assembly. The wall roughness was specified as 7 μm (276 μ-inches), and the default wall thermal condition was set as adiabatic because the focus of the study was pressure drop and flow distribution rather than heat transfer. The inlet boundary condition was applied at the top of the left manifold as a mass flow inlet of 0.25 kg/s (3.96 GPM). The outlet boundary condition was applied at the top of the second manifold as an environmental pressure outlet of 101.325 kPa (14.696 psi) at 293.2 K (527.76 °R). The primary simulation goals were the average inlet pressure, average outlet pressure, and total pressure drop across the panel according to Equation 9. The same general setup was applied to all 4 design assemblies so that the results could be compared directly.

$$\Delta P = P_{in,avg} - P_{out,avg} \quad (9)$$

The CFD results were evaluated using both quantitative pressure-drop values and qualitative contour plots. Pressure contours were used to identify high-pressure and low-pressure regions along the manifold, while velocity contours were used to determine whether flow was evenly distributed across the panel or concentrated in specific regions. This was important because the best design was not necessarily the one with the lowest pressure drop; it also needed to provide maintain or improve heat transfer through the panel. The baseline design (B1-B1) served as the reference case. The optimized designs were then compared against each other and the baseline to determine how changing the hole spacing and outlet configuration improved the flow behavior.

Based on the pressure drop and velocity contour analysis, the performance of the three model configurations is summarized below:

- C1-Open: This configuration was identified as the most effective design. It achieved the lowest pressure drop at 789 Pa (0.114 psi) and demonstrated the most uniform velocity distribution across the tubes (figures A.7 and A.8).

Copyright © 2026 by ASME

- C1-C1: This configuration showed a mid-range performance with a measured pressure drop of 819 Pa (0.119 psi) (figures A.3 and A.4).
- C1-B1: This configuration was the least successful in meeting design requirements. It produced the highest pressure drop at 860 Pa (0.125 pounds per square inch) and exhibited the greatest velocity variations (figures A.5 and A.6).

However, while discussing the results with our sponsor, it was noted that the system sometimes reverses the direction of the flow, leading the outlet manifold to act as an inlet, and vice versa for the inlet. Given this information, our recommendation was to use the C1-C1 panel assembly as the best choice.

Overall, CFD played a major role in the design process by allowing the team to compare manifold concepts before manufacturing. The analysis confirmed which designs were on the right track and provided an idealized reference for interpreting physical testing results. However, simulations do not fully capture all manufacturing effects, such as drilled-hole burrs, fixture alignment error, drill wander, or RTV silicone that was used in real life to seal the gaps and connect the assemblies. Therefore, a more complete CFD verification study would require mesh refinement and mesh convergence study.

Manufacturing

Polyvinyl chloride (PVC) pipes were selected for the manifold prototypes due to their cost-effectiveness and availability. The sponsor provided a 1066.8 x 1270 x 6.35 mm (42 x 50 x 0.25 in) panel consisting of 6.35 mm (1/4 in) pipes, which was cut into four identical sections to accommodate the four proposed designs (Appendix D, Figure D5). Each model was scaled to 50% of the original assembly to streamline manufacturing and testing as these smaller units are easier to swap. PVC sheets were used to mimic the layer connecting the manifold to the panel tubes.

The manifold caps were 3D printed using PLA for its durability and accessibility. The top caps were printed at 100% infill for maximum solidity because they were intended to hold garden hose pipe fittings, while the bottom caps were printed at 40% infill. To assemble the components, RTV silicone sealant was chosen for its high durability, flexibility, and waterproof properties. Additionally, a steel brush was used to clean the interior of the PVC pipes, ensuring the orifices remained clear of debris. This prevented unintentional 're-entrant' flow scenarios, where internal burrs or debris perturb the fluid discharge.

An estimated cost of the production of all assemblies can be approximated to $4,949.47 as seen by adding the total costs of all material purchased, PLA used, and manufacturing time spent by team members at $100 per hour costs seen in Tables 2, 3, 4, and 5. The total cost of development time spent can be estimated to be $28,200 as seen in Table 6.

To scale manufacturing to 1,000 models, the main change that could improve build time would be to ensure no air bubbles or space remain between the layers connecting the manifold to the panel by using the correct tool. The first 3 prototypes had much worse adhesion and were prone to become undone around the area where the layer met the panel because the RTV was manually applied with no tools. This led to an increase in build time spent on each panel as they needed to get fixed. The only way to effectively seal everything was by taking off the first layer of RTV in that area and applying it with a scraper to fill in all empty spaces between the panel and the layer.

Table 2: Estimated Material Costs

Item	Quantity	Total Cost
1-1/4 Inch PVC Pipe	12	$191.4
1/8-Inch-Thick PVC Sheet	1	$30.99
Replacement 1/8-Inch-Thick PVC Sheet	2	$29.82
Waterproof RTV Silicone Sealant (Pack of 10 units)	1	$62.99
1-1/4 Inch Steel Brush	1	$8.51
Husky Water hose	2	$39.96
Total Material Costs		$363.67

Table 3: Estimated Sponsor Provided Material Costs (not considering time of manufacturing)

Item	Quantity	Total Cost
1066.8 x 1270 x 6.35 mm Polypropylene Panel	1	$29.44
Sponsor Provided Material Cost		$29.44

Table 4: Estimated 3D Printing Costs using $0.1 per gram

Item	Quantity (per unit)	Number of Units	Total Cost
PLA 100% Solid Caps	51.16g	8	$40.93
PLA 40% Solid Caps	19.29g	8	$15.43
Total 3D Printing Cost			$56.36

Table 5: Estimated Manufacturing Time Costs

Member	Hours	Total Cost
Marcela Hinojosa	20	$2,000
Abdulwahab Sayes	15	$1500
LloydAnthony Blackwood	7	$700
Boris Lokossou	13	$1,300
Total Manufacturing Cost		$4,500

Copyright © 2026 by ASME

Table 6: Estimated Development Costs

Member	Hours	Total Cost
Marcela Hinojosa	85.5	$8,550
Abdulwahab Sayes	78.5	$7,850
LloydAnthony Blackwood	65	$6,500
Boris Lokossou	53	$5,300
Total Development Cost		$28,200

TEST PLAN AND RESULTS

To begin testing, a sump pump was connected to the manifold assembly. The pump was powered via a VARIAC set to 65% voltage to regulate the flow rate and prevent the models from experiencing excessive pressure that could lead to structural failure. The procedure involved first running cold water through the models to establish a thermal baseline, followed by the introduction of hot water to simulate operating conditions.

The discharge was directed into a collection basin to measure outflow, while the model itself was housed within a secondary basin. This secondary containment allowed for the collection of any leaks, which were measured and compared against the primary outflow to validate the accuracy of the discharge data. During the hot water phase, thermal images were captured at the beginning, middle, and end of the cycle to track heat distribution. The reservoir temperature was also recorded throughout the process to allow for data normalization during later analysis. The specific hardware configuration, including VARIAC, ammeter, reservoir, and pressure gauges, is detailed in Appendix D, Figure D6.

The first test quantified the flow improvement achieved by deburring the manifold (Appendix D, Figure D2). According to fluid mechanics principles, the geometry of an orifice's entrance directly affects its discharge coefficient. Table 7 compares the burred and deburred manifolds after a steel brush was run through the interior for five minutes. During testing, the manifold was filled with water, and the discharge time was tracked specifically for the final orifice, while all other orifices remained plugged.

Table 7: Time for flow to come out of each burred or deburred orifice

	Burred	Deburred
1	42.65 secs	41.75 secs
2	41.56 secs	41.70 secs
3	42.75 secs	41.33 secs
4	42.19 secs	41.42 secs
5	41.47 secs	40.72 secs
Mean	42.124 secs	41.38 secs

These initial results showed an improvement of only 1.8%, which may be inaccurate due to insufficient cleaning of the manifold models, as seen in Appendix D, Figure D2. A subsequent test was performed using 3D-scale models with identical manifold and orifice diameters. This test compared a standard clear orifice against a re-entrant orifice of the same length as the orifice diameter, which resulted in a significant 26% improvement in flow. However, the results remain inconclusive as more testing is needed to determine whether cleaning the manifold is truly beneficial.

The second test utilized thermal imaging to capture temperature variations across the panels and quantify improvements in heat transfer. To establish a baseline, the models were first filled with cold water to lower their temperature below the ambient environment. Hot water was then introduced and pumped through the system; the panels were allowed to reach a steady state, which occurred within approximately two minutes, before final thermal data was recorded.

Table 8: Temperature Variation Across Panel

Designs	Mean [˚C]	Standard Deviation [˚C]	Max [˚C]	Min [˚C]	Coefficient of Variation
B1 – B1	19.11	3.98	27.75	8.95	0.2083
C1 – B1	14.88	2.17	19.61	11.03	0.1458
C1 – C1	14.93	3.37	21.5	9.08	0.2261
C1-Open	15.85	2.72	20.09	9.91	0.1719

The above table, Table 8, shows the key temperature characteristics across the panel for four separate thermal imaging test. It shows the average temperature, standard deviation of temperature, maximum and minimum temperature, and coefficient of temperature variation across each panel. The lower the coefficient of temperature variation correlates to a more even temperature distribution across the panel. Another phase of testing was done to validate the previous data (see Appendix D, Table 13). From that test C1-B1 leaked so the data cannot be considered. Model C1-OPEN had a higher coefficient of variation than the previous test, implying that it transfers heat less efficiently than the baseline model. Model C1-C1 in this round of testing showed a 16% improvement in heat transfer compared to the baseline, which is in line with expected results.

$$Coefficient\ of\ Variation = \frac{Standard\ Deviation}{Mean} \quad (7)$$

Table 9: Pressure Drop results

Designs	ΔP (kPa)	ΔP (kPa)	ΔP (kPa)	Mean ΔP (kPa)
B1 - B1	2.5	2	2	2.17
C1 - B1	1.3	1.6	1.4	1.43
C1 - C1	1.4	1.8	1.8	1.67
C1 - Open	2	1.9	2	1.97

Copyright © 2026 by ASME

Table 9 presents the measured pressure drop across each model in kilopascals (kPa). For the final testing phase, pressure gauges were attached to the inlet and outlet hoses, with a single operator manually applying pressure to ensure a proper seal. According to these results, Concept 2 (C1–B1) demonstrated the most significant reduction in pressure drops. However, the data recording process was complicated by sealing issues at the inlets and outlets, necessitating manual human intervention to maintain consistent internal pressure during the readings.

Table 10: Flow leaving each panel system with leaks as errors

Designs	Flow out (kg)	Flow out (kg/s) - in 5 mins	Leaks (kg)	Leaks/Flow out
B1 - B1	59.30	0.198	3.9	6.5%
C1 - B1	53.61	0.179	4.7	8.7%
C1 - C1	62.71	0.209	2.2	3.5%
C1 - Open	56.86	0.190	4.1	7.2%

Table 10 details the flow rates and associated leakages for each design concept. The trustworthiness of the flow rate capture varies across the models due to the manual assembly of the PVC and RTV silicone seals. Concept 2 (C1–C1) is the most reliable data set, exhibiting the lowest leak-to-flow ratio at 3.5%. This high level of integrity suggests that the recorded flow rate of 0.209 kg/s is a highly accurate representation of the design's performance.

Conversely, Concept 1 (C1–B1) showed the highest error margin with an 8.7% leakage rate. While this indicates a higher degree of uncertainty, the overall data across all four models remains valuable for identifying trends. Despite the leaks, the data clearly identifies Concept 2 (C1–C1) as the superior design, as it achieved the highest outflow (0.209 kg/s) while maintaining the most secure structural seals. This suggests that the C1–C1 configuration not only optimizes flow but may also experience less internal backpressure, thereby reducing the stress on the manifold's mechanical joints.

Using the relationship between pressure drop and volumetric flow, the pumping power for each design was calculated (Equation 8) for a 24/7 monthly operating cycle at the local Monroe County electricity rate of $0.17/kwh.

$$Power\ (Watts) = \Delta P \cdot Q \quad (8)$$

Table 11: Power Improvement

Designs	Power (Watts)	Power Improvement
B1 - B1	0.430	---
C1 - B1	0.256	40.47 %
C1 - C1	0.349	18.84 %
C1 - Open	0.374	13.02 %

Concept 1 (C1–B1) emerged as the most energy-efficient, offering a 40.47% reduction in power consumption compared to the baseline. Even the most conservative improvement (Concept 3, C1-Open) suggests a 13.02% reduction in energy draw, confirming that manifold optimization directly impacts the customer's bottom line and carbon footprint.

Table 12: Designs final evaluation

Designs	Lower Pressure drop by ≥ 5%	Lower Pumping Power	Maintain or Improve Heat Transfer	Below Material Endurance Limit
C1 - B1	Pass	Pass	Pass	Pass
C1 - C1	Pass	Pass	Fail	Pass
C1 - Open	Pass	Pass	Pass	Pass

The final design selection was based on a 'Pass/Fail' matrix across the four specification performance metrics (Table 12). The conclusion shows that C1-C1 fails in the criteria of maintaining or improving heat transfer, while C1-B1 and C1-Open passed all specifications: reducing pumping power while maintaining or improving heat transfer efficieny. Therefore, based on the testing data, C1-B1 ranks first followed by C1-Open as recommendations for MicroEra's next-generation heat exchangers. Both designs remained well below the material endurance limits of the PVC and RTV assembly, ensuring that the 50% scale findings can be safely increased to full-scale manufacturing.

INTELLECTUAL PROPERTY

Even though the design optimizes the uniformity of flow across the panel, and decreases the pressure drop, generally it follows the same setup as MicroEra. Hence, the design is not patentable; it is an optimization of an already existing MicroEra idea.

An existing patent within this field is US10175669B2 which is a Fluid control measuring and controlling device. The invention aimed at optimizing the flow on numerous pipes through controlling the velocity using sensors. This design would not be applicable to our problem for two reasons:

1. It doesn't consider the manifold (which is where the invented device is supposedly placed).
2. One of the primary requirements is that we are only allowed to work on the spacing and sizing of the orifices to optimize the flow without altering any other geometry.

SOCIETAL AND ENVIRONMENTAL IMPLICATIONS

MicroEra's THERMAPlus™ system has a large positive environmental impact being the reduction of carbon emissions in buildings who account for 1/3 of global carbon emissions [1].

Copyright © 2026 by ASME

This technology works to save commercial buildings and campus/district energy systems capital by reducing their respective energy costs over the product's lifespan. These carbon reductions happens when the respective customers offset their heating or cooling to respective to the THERMAplus™ system during peak hours when the cost of energy is the highest and when peaker plants [2] might be active. Over time, this system will offset a large amount of carbon and save its users a large amount of capital over the full life cycle of the product.

Additionally, the THERMAplus™ system adds to grid flexibility by pairing well with intermittent renewable sources like wind and solar by reducing electricity demand during peak hours. Furthermore, if this technology is adopted on utility scale, it will aid in reducing the cost of electricity during peak hours saving consumers millions and giving utilities more tools at their disposal during extreme weather events [3] to reduce load shedding and blackouts.

The materials process used to manufacture the THERMAplus™ system includes the plastic, polypropylene which requires an energy intensive manufacturing process [4]. The alternative to polypropylene is copper which has a larger carbon footprint, and unlike polypropylene does not sequester carbon [9]. The volume of polypropylene used in the system is not large, though not unsubstantial, and a fully developed recycling program will mitigate much of the environmental impact of improper waste disposal of the material at the end of the product's life cycle. Furthermore, the carbon offset the system will achieve far outstrips any environmental impact during the manufacturing process, enabling the THERMAplus™ system to have a net positive carbon footprint over the course of its life cycle.

RECOMMENDATIONS FOR FUTURE WORK

If there were 6 additional months to work on the project, the main priority to focus on would be on running the testing procedure additional times to ensure less variability in the results. As the testing procedure was being set up, multiple, uncontrollable variables such as leakage, limited hot water reservoirs, and outside temperatures presented themselves as obstacles and time had to be spent trying to mitigate their effects on the results. By the time a testing procedure that dealt with these issues was made, there was very limited time left to conduct proper testing. Spending more time conducting tests would ensure that the thermal and fluid analysis results are clear and constant, which is critical for determining if the proposed optimized design is worth the cost of a new production process.

Moreover, the MATLAB code produced for a Pressure Drop Calculator could not be optimized after a certain point due to time constraints. The first version of the MATLAB code made to calculate the pressure drop across one of the panels of the heat exchanger device overlooked the mass conservation of the fluid, which meant that it would not fully represent the flow behavior through the panel. A second version of the code was promptly made, but due to the limitations of the chosen MATLAB solver, the results of only 5 out of 21 orifices could be made. Further research on MATLAB solvers and optimization of the code could lead to better representations of physical results that could be obtained mathematically when changing the orifice configuration.

Furthermore, a more detailed manufacturing procedure could be developed as small variations in the production of the assemblies due to human errors were visible during testing as the sealant ripped due to the inadequate sealing of empty space between the layers and panels. A more straightforward manufacturing process can reduce these variations and errors. It was observed that drilling the holes with a milling machine while on a slow gear or with a dull drill bit causes mayor development of burs on the orifices, which can perturb flow, and is something to prevent in future manufacturing practices.

In addition, members of the team had to learn a new type of CFD analysis that is not part of the class curriculum called CFD Designer in Siemens NX. A lot of time was spent trying to master this application as it required less computational power, which gave faster and accurate results. The main problem was the lack of accessible resources that showed how to change the boundary conditions within the whole panel assembly. Additional time could aid in mastering CFD Designer, which would allow the team to produce better models.

ACKNOWLEDGMENTS

We want to take a moment to acknowledge everyone that helped make this project possible.

We would like to thank our contact with MicroEra Power, Molly Over, as she provided continuous support and feedback on our ideas. We are also thankful for the time Molly took out of her day to provide us with sample manifolds and panels that we used as references for our CAD models.

We would also like to show our gratitude to Lab Specialist Samantha Kriegsman for her assistance with what materials we should use and for all the help she provided with our testing set up every time we ran our testing process.

We would like to express our deep gratitude to Professor Ibrahim Mohammad and PhD student Yasser Abdelshafy, who spent a lot of time assisting us with our MATLAB code and general understanding of fluid dynamics that allowed us to optimize our Pressure Drop Calculator.

We would like to show our appreciation towards Christine Pratt for her assistance in getting crucial tools used during testing and for her valuable help in setting up our testing process.

We would also like to express our gratitude to Jim Alkins for providing advice on how to set up our testing and for allowing us to use the workplace in Rettner hall to work.

We would like to thank Bill Mildenberger for his general assistance in Taylor Hall and for allowing us to use the machinery there.

We are also thankful to Senior Lab Engineer Clair Cummingham from the Chemical Engineering department for providing extremely useful tools such as pressure gauges and insight into how we could use these tools to get the results we wanted.

 Copyright © 2026 by ASME

We would like to show our appreciation to Senior Lab Engineer Edward Herger who gave us valuable advice as to how to measure power and pressure throughout the system.

We would like to express our deep appreciation towards Teaching Assistant Kyle Christensen for all his time and guidance he has given us throughout the semester. We are also thankful for his quick response time and for his urgency when ordering our assembly materials.

We want to express our immense gratitude towards Professor Christopher Muir, who always directed us to the right path, taught us how to properly set up CFDs, and gave us the knowledge needed to complete this project. We are forever thankful for all the time he has spent meeting with us to answer our inquiries and for helping us find solutions for our problems.

REFERENCES

[1] Lu, M., and Lai, J., 2020, "Review on Carbon Emissions of Commercial Buildings," *Renewable and Sustainable Energy Reviews*, 119, p. 109545, https://doi.org/10.1016/j.rser.2019.109545.

[2] Clean Energy Group and Strategen, 2022, *The Peaker Problem: An Overview of Peaker Power Plant Facts and Impacts in Boston, Philadelphia, and Detroit*, Clean Energy Group, https://www.cleanegroup.org/wp-content/uploads/The-Peaker-Problem.pdf.

[3] Gonçalves, A. C. R., Costoya, X., Nieto, R., and Liberato, M. L. R., 2024, "Extreme Weather Events on Energy Systems: A Comprehensive Review on Impacts, Mitigation, and Adaptation Measures," *Sustainable Energy Research*, 11(1), p. 4, https://doi.org/10.1186/s40807-023-00097-6.

[4] Hossain, M. S., Rahman, M. T., and Hasan, M. M., 2021, "A Review of Hybrid Renewable Energy Systems: Architectures, Optimization and Applications," *Sustainable Energy Technologies and Assessments*, 44, p. 101011, https://doi.org/10.1016/j.seta.2020.101011.

[5] PVC Fittings Online, n.d., "Strength of PVC Pipe (With Strength Chart)," https://www.pvcfittingsonline.com/blogs/resource-center/strength-of-pvc-pipe-with-strength-chart.

[6] Budynas, R. G., and Nisbett, J. K., 2015, Shigley's Mechanical Engineering Design, 10th ed., McGraw-Hill Education, New York, p. 290.

[7] Budynas, R. G., and Nisbett, J. K., 2015, Shigley's Mechanical Engineering Design, 10th ed., McGraw-Hill Education, New York, p. 433.

[8] Xometry, 2024, "Polypropylene vs. PVC: Differences and Comparisons," https://www.xometry.com/resources/materials/polypropylene-vs-pvc/

[9] Community Engineering Services, n.d., "Embodied Energy: Polypropylene vs. Copper," https://coengineers.com/embodied-energy-polypropylene-vs-copper/.

Copyright © 2026 by ASME

APPENDIX A – CFD RESULTS

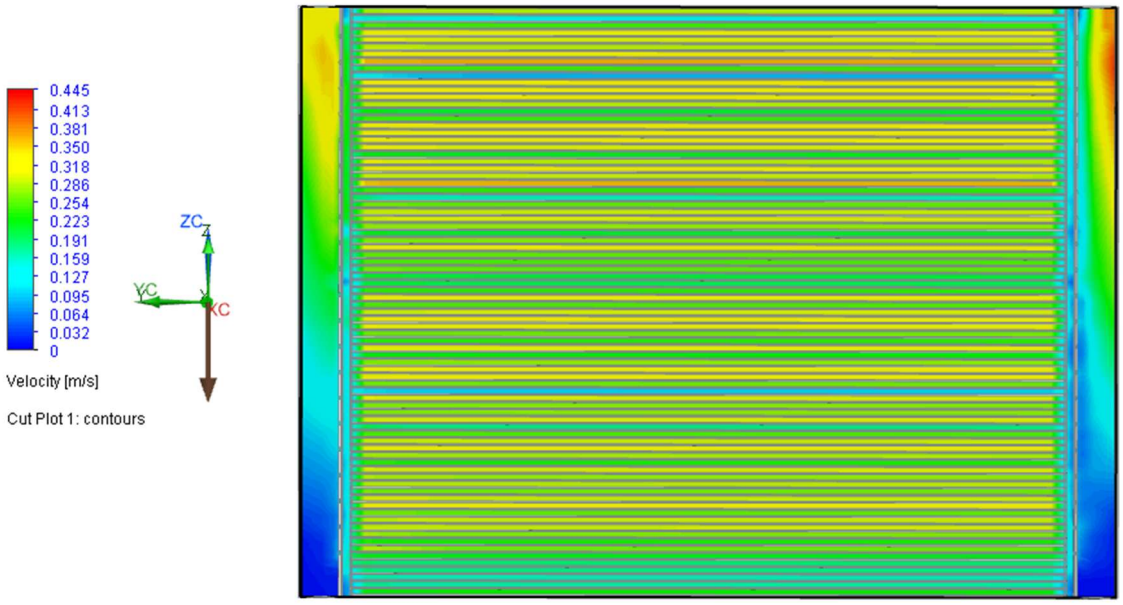

Figure A.1 shows the CFD velocity flow of water across the panel in the Baseline design.

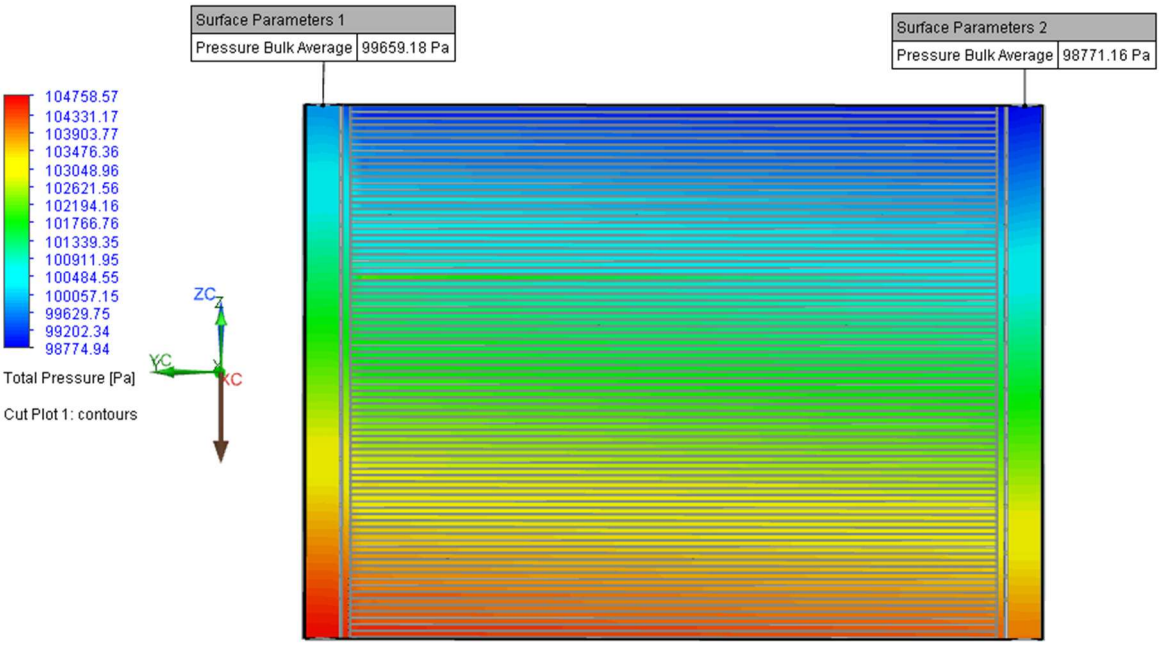

Figure A.2 shows the CFD total pressure variation across the panel in the baseline design. Note the inlet and the outlet pressure values at the top of each manifold; these values were used to compute the theoretical pressure drop.

Copyright © 2026 by ASME

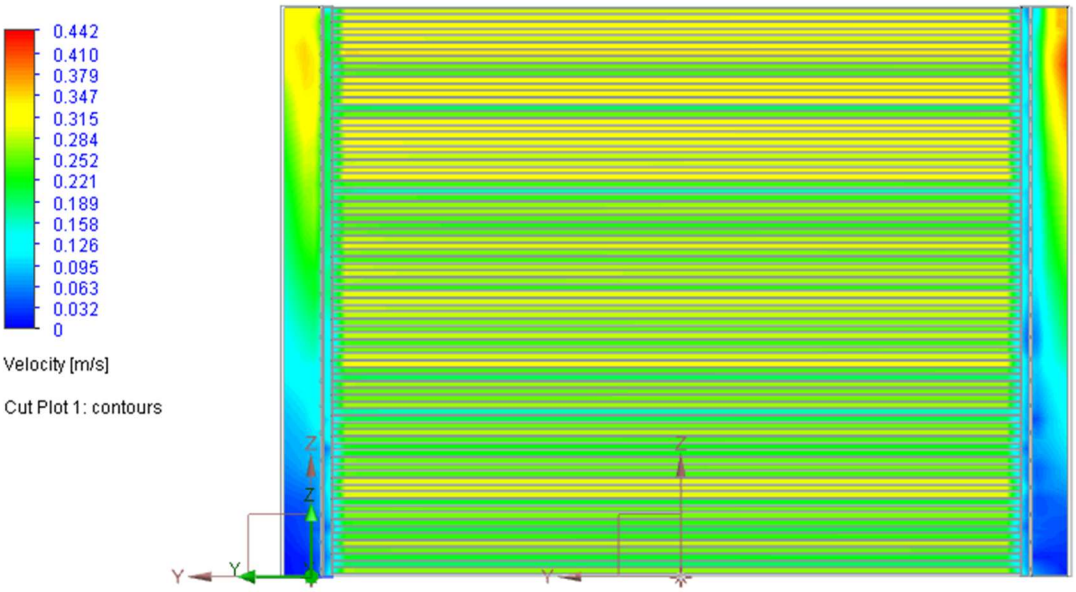

Figure A.3 shows the CFD velocity flow of water across the panel in the optimized-optimized manifolds design.

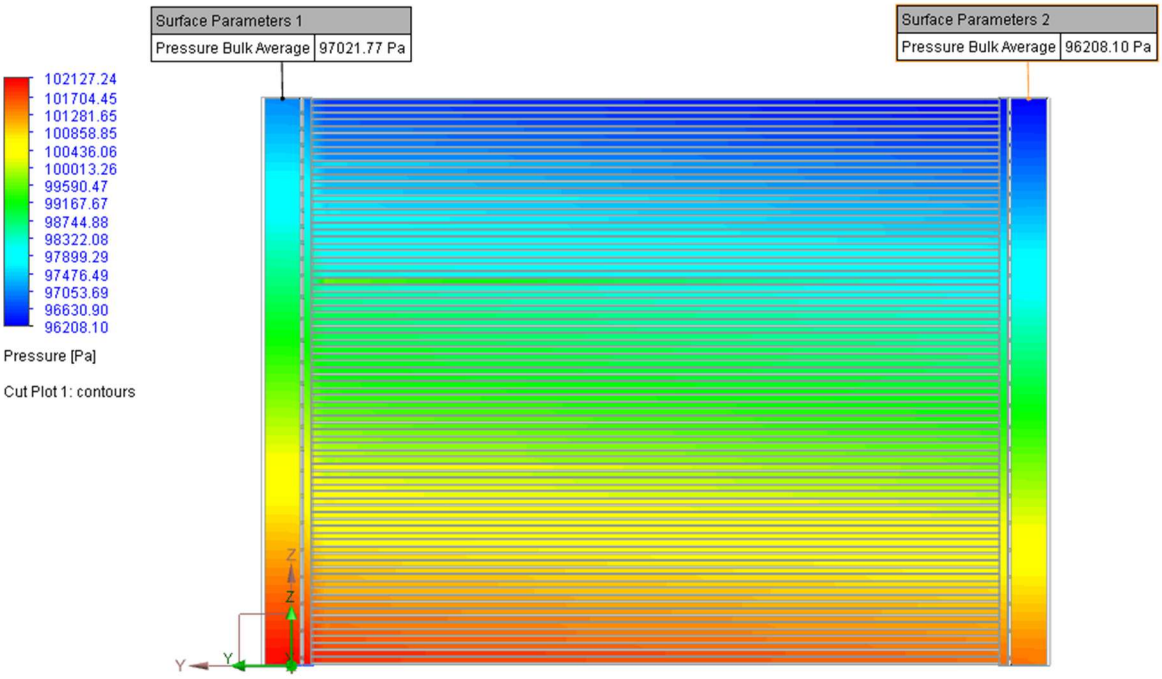

Figure A.4 shows the CFD total pressure variation across the panel in the optimized-optimized manifolds design. Note the inlet and the outlet pressure values at the top of each manifold; these values were used to compute the theoretical pressure drop.

Copyright © 2026 by ASME

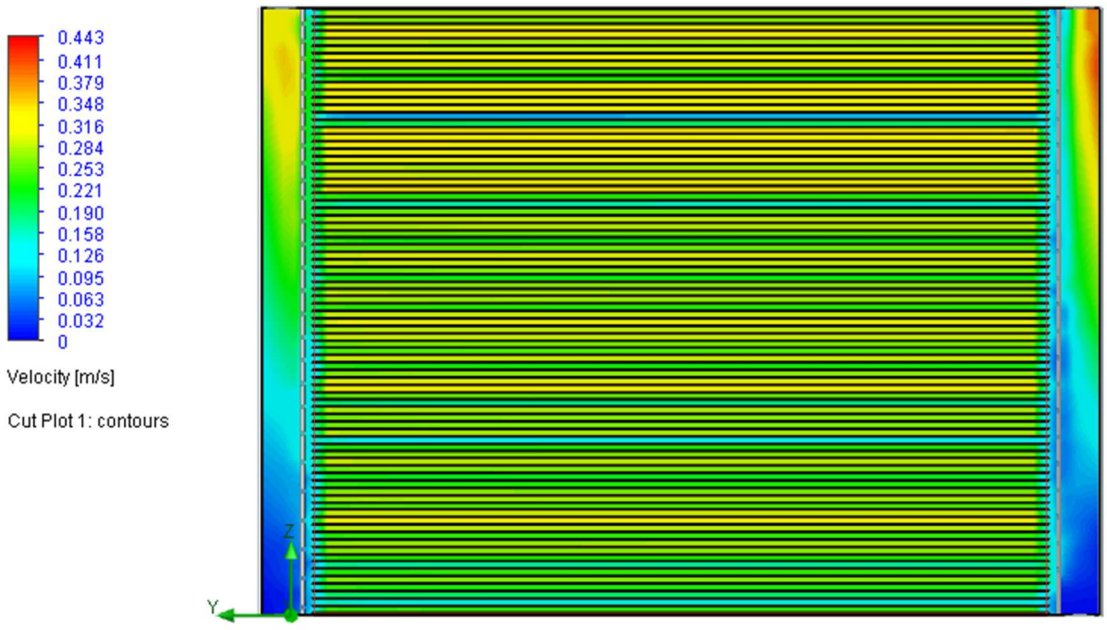

Figure A.5 shows the CFD velocity flow of water across the panel in the optimized-baseline manifolds design. The optimized manifold is on the left (as the inlet), and the baseline manifold is on the right (as the outlet).

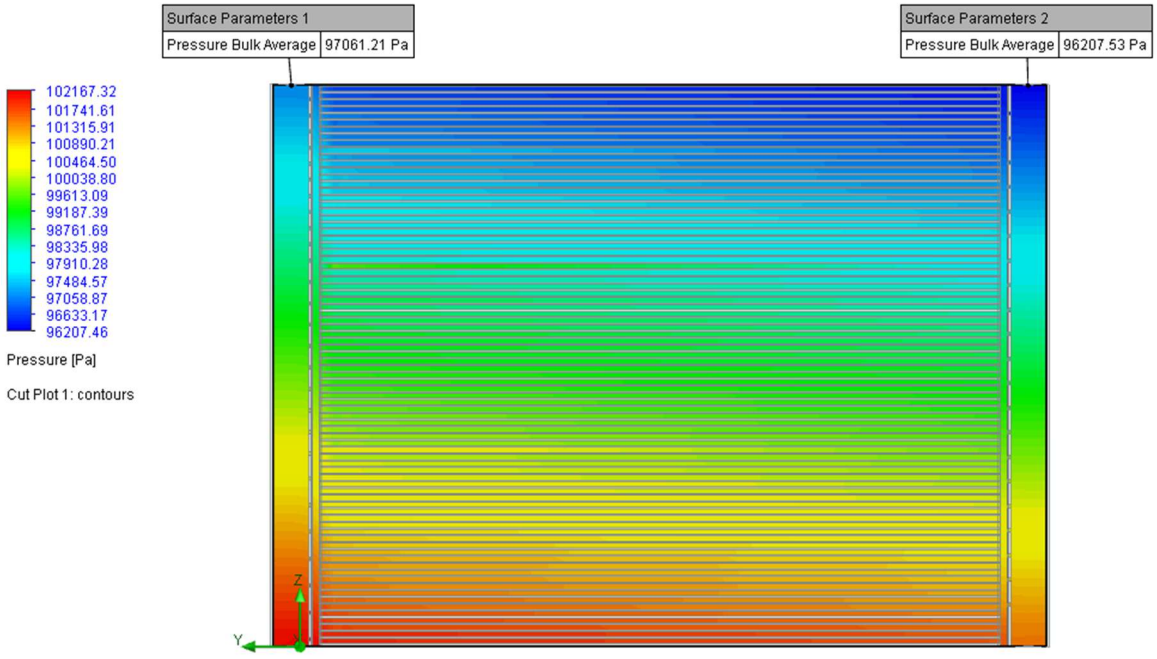

Figure A.6 shows the CFD total pressure variation across the panel in the optimized-baseline manifolds design. Note the inlet and the outlet pressure values at the top of each manifold; these values were used to compute the theoretical pressure drop.

Copyright © 2026 by ASME

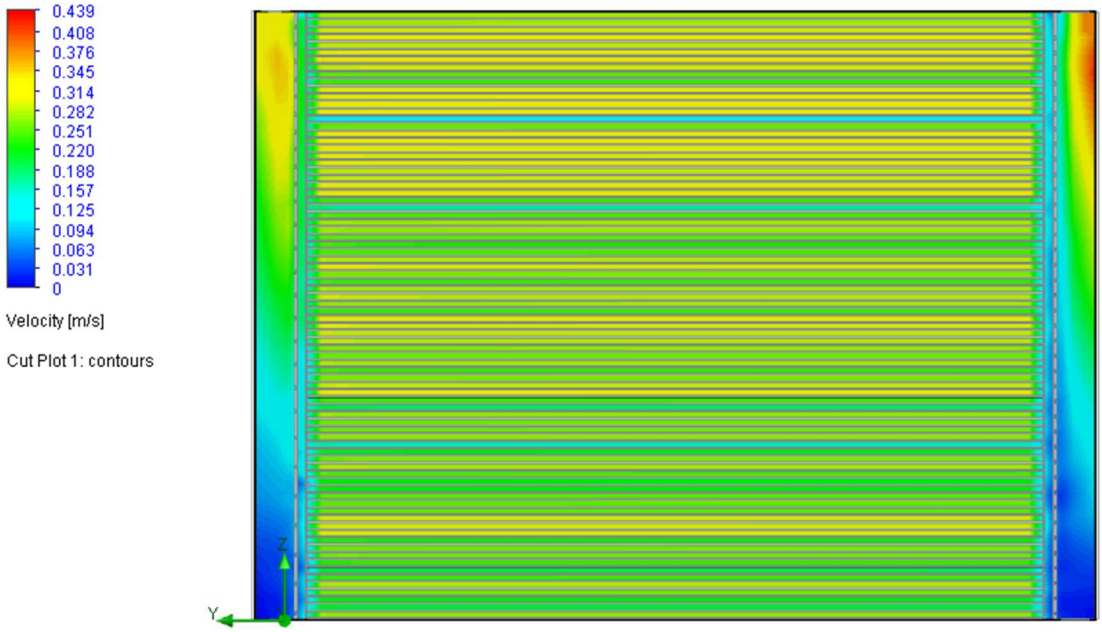

Figure A.7 shows the CFD velocity flow of water across the panel in the optimized-open manifolds design. The optimized manifold is on the left (as the inlet), and the open manifold is on the right (as the outlet).

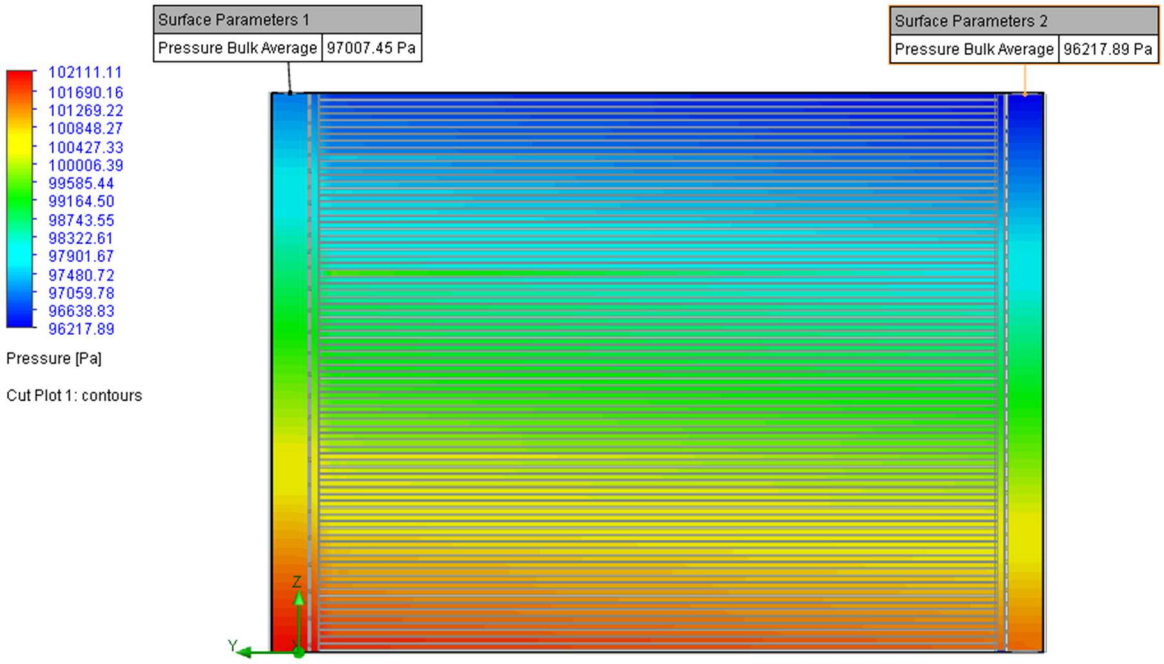

Figure A.8 shows the CFD total pressure variation across the panel in the optimized-open manifolds design. Note the inlet and the outlet pressure values at the top of each manifold; these values were used to compute the theoretical pressure drop.

Copyright © 2026 by ASME

APPENDIX B – CAD DRAWING PACKAGE:

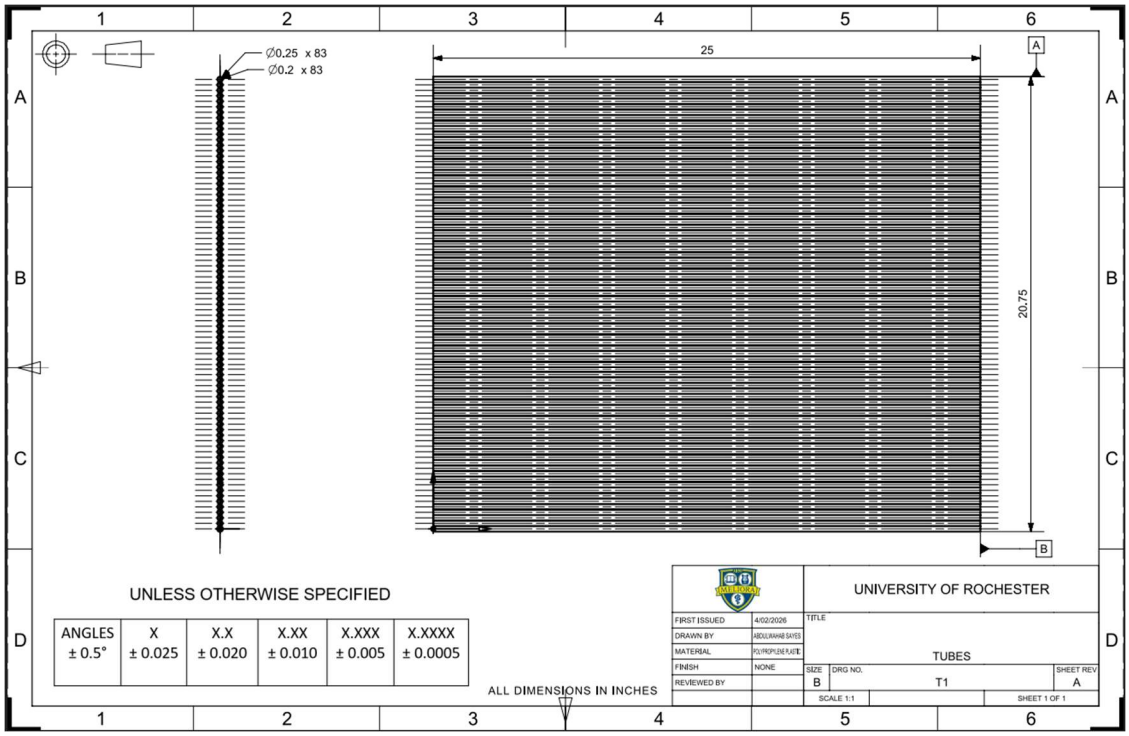

Figure B.1 shows CAD drawing of the tubes used to connect the two manifolds together.

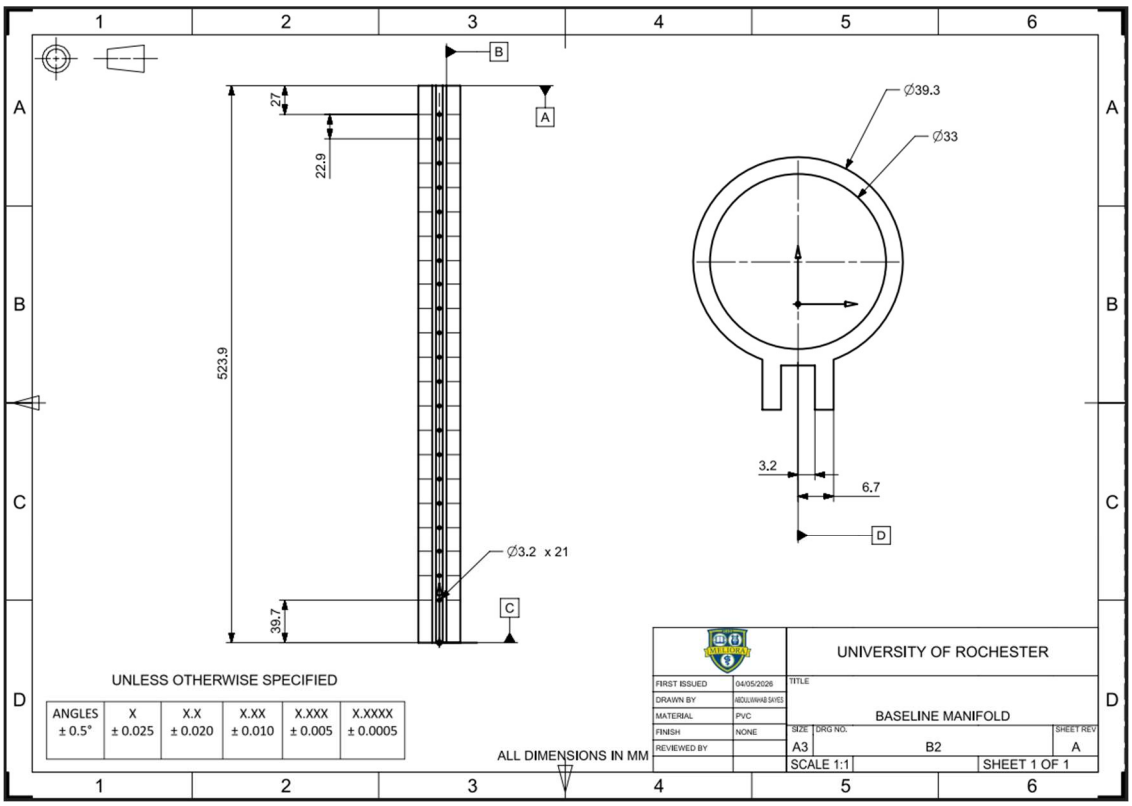

Figure B.2 shows the baseline manifold design used in CFD and for manufacturing the testing part.

Copyright © 2026 by ASME

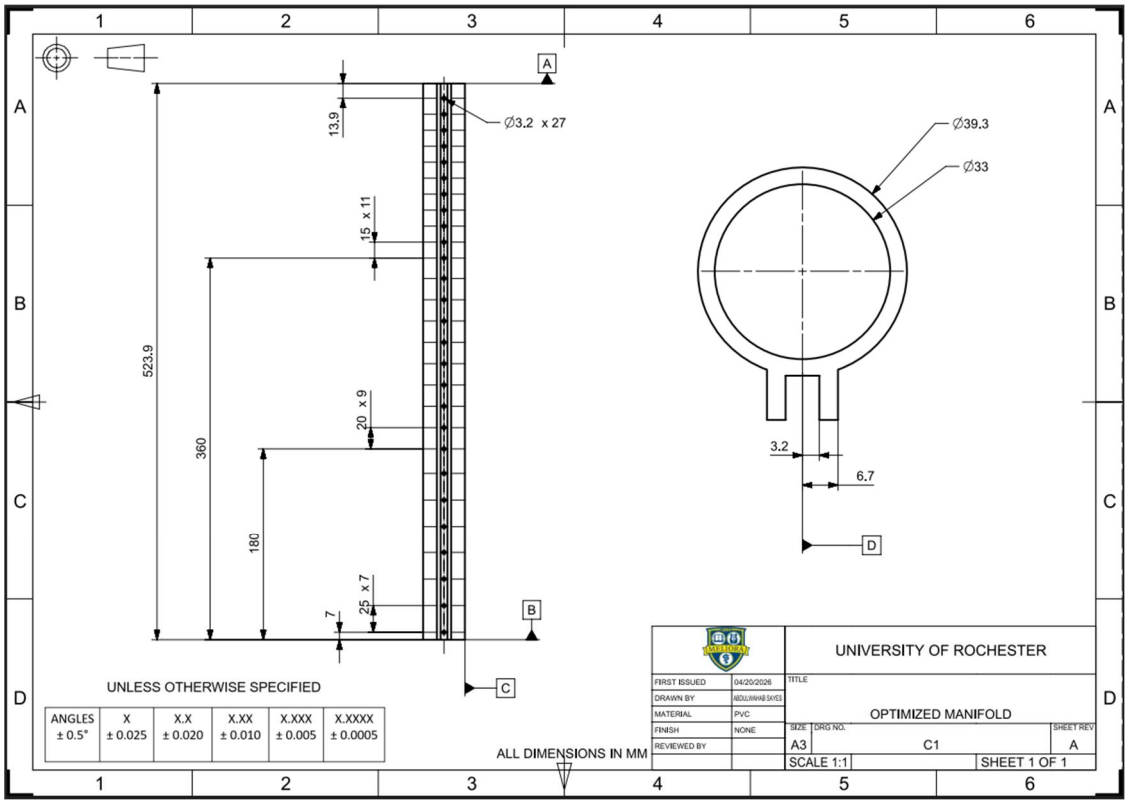

Figure B.3 shows the optimized manifold design. Note the three different spacings between the holes in zone A, B and C.

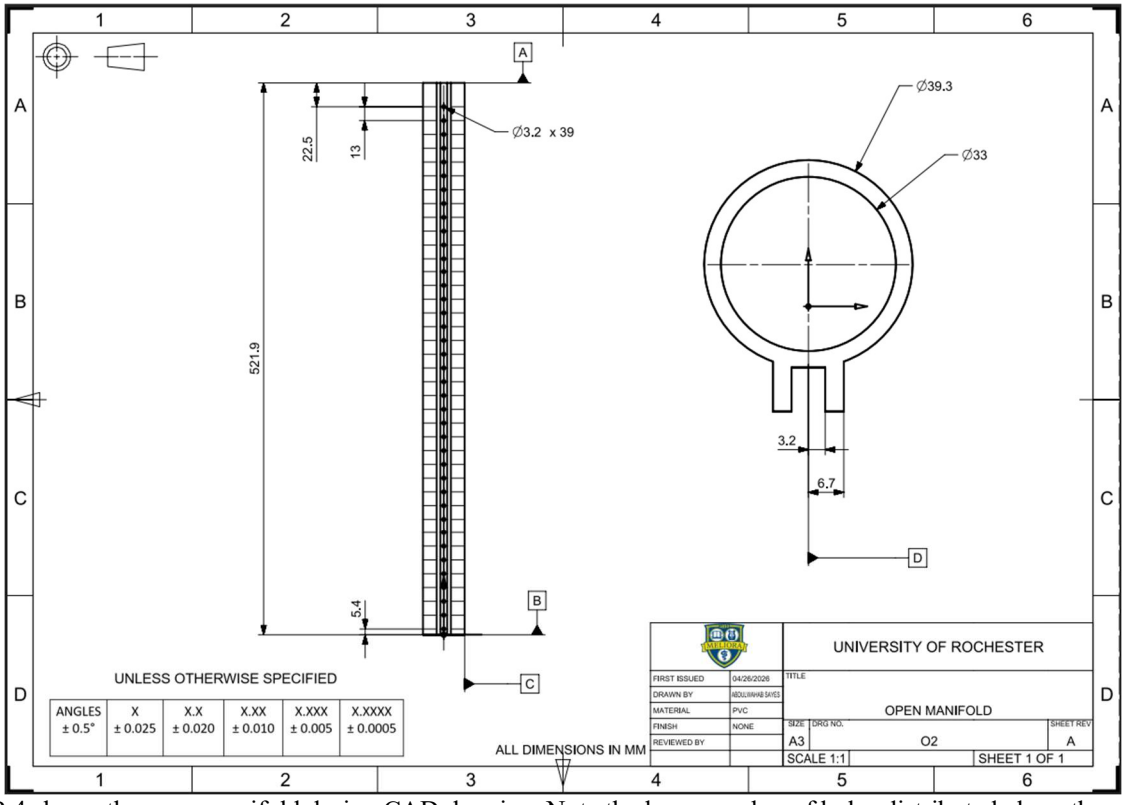

Figure B.4 shows the open manifold design CAD drawing. Note the large number of holes distributed along the manifold.

Copyright © 2026 by ASME

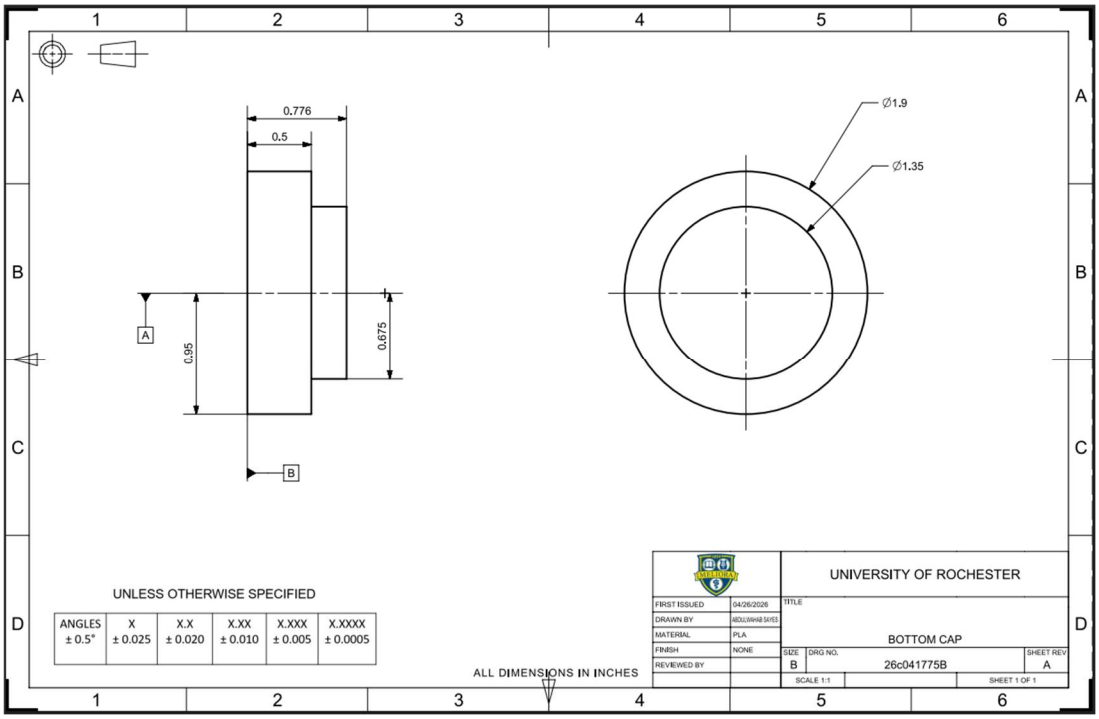

Figure B.5 shows the bottom cap used to seal the manifold. During physical testing, RTV silicone was used for waterproofing the 3D printed part.

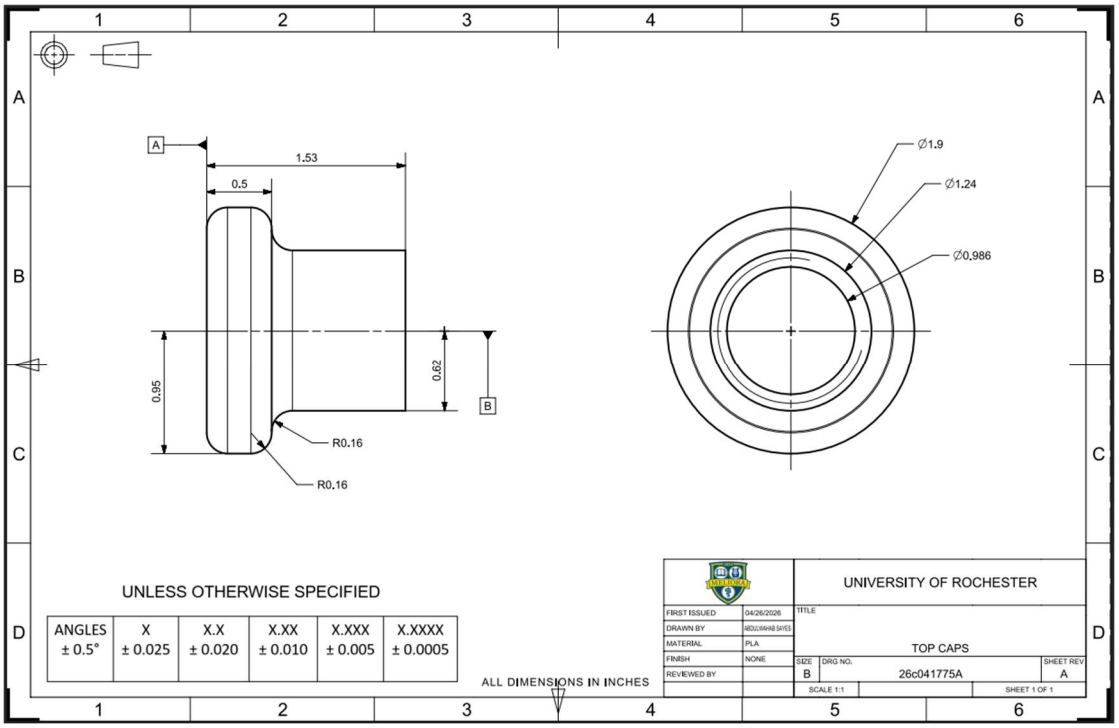

Figure B.6 shows the Top caps used to seal the hose on the inlet and the outlet manifolds.

Copyright © 2026 by ASME

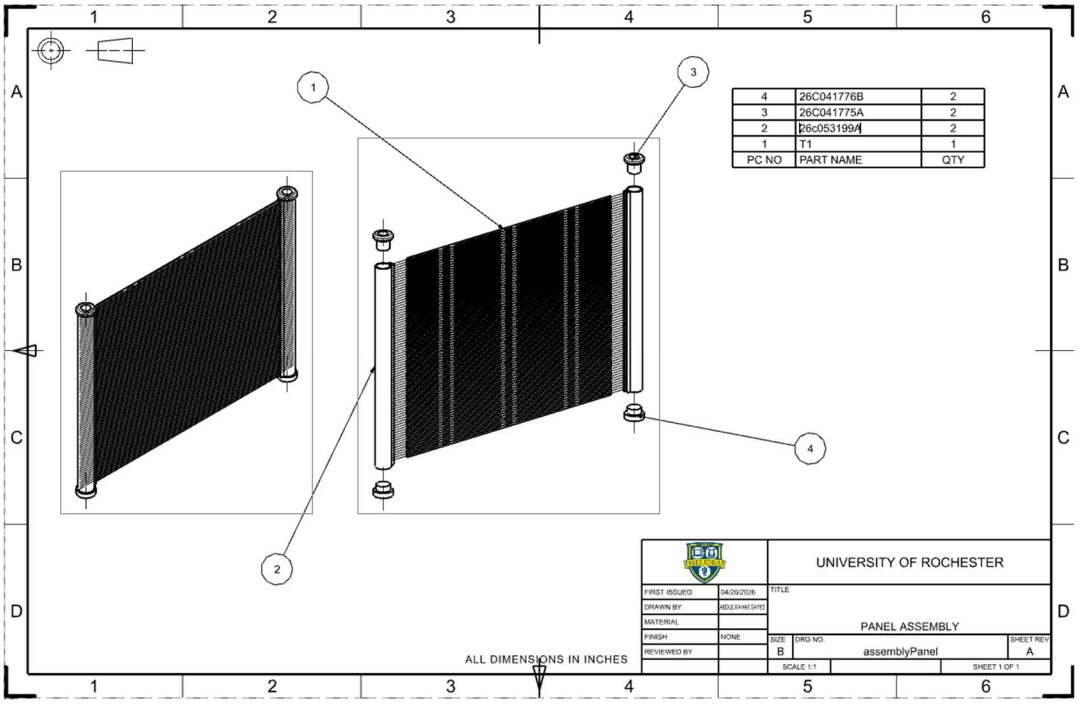

Figure B.7 shows the full assembly of the panel. The manifold designs would replace part 2.

Copyright © 2026 by ASME

APPENDIX C – THERMAL ANALYSIS

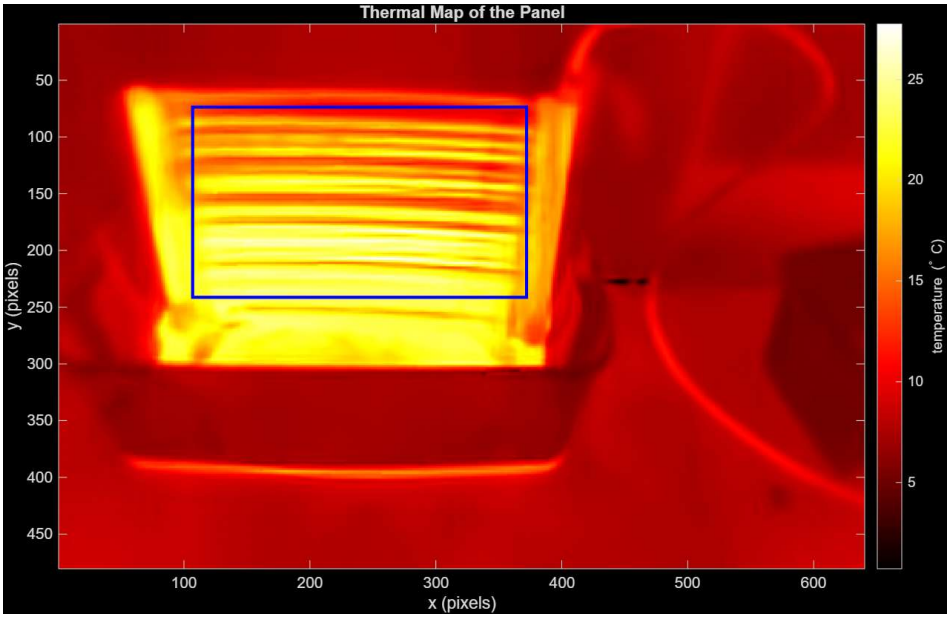

Figure C1 shows the Baseline Inlet to Baseline Outlet Thermal Image and region of interest.

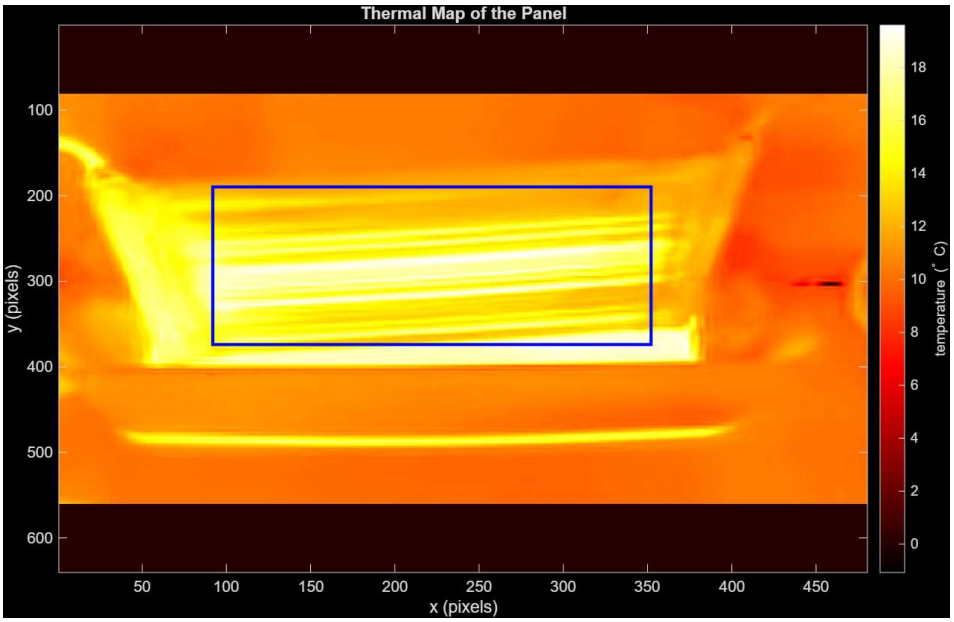

Figure C2 shows the Concept One Inlet to Baseline Outlet and region of interest.

Copyright © 2026 by ASME

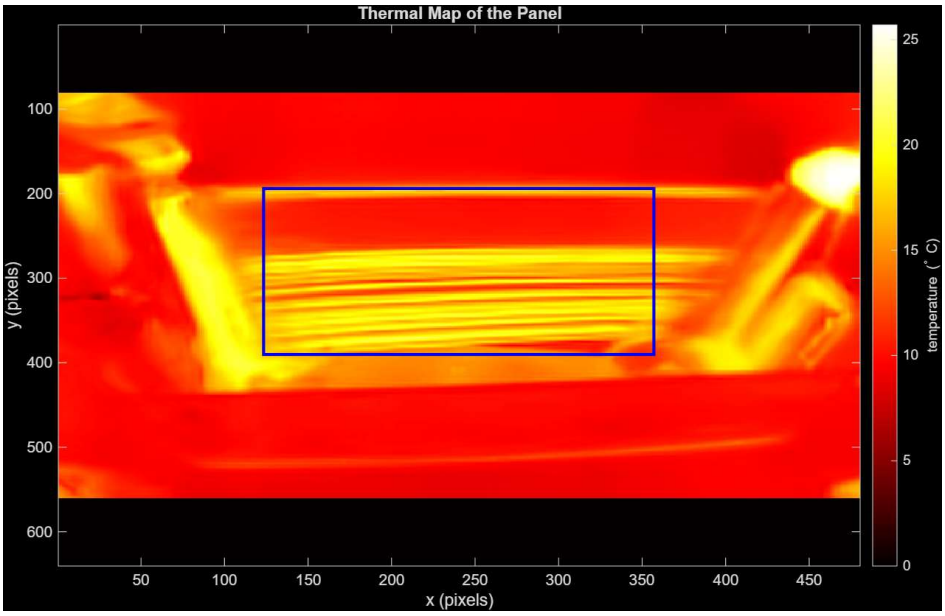

Figure C3 shows the Concept One Inlet to Concept One Outlet and region of interest.

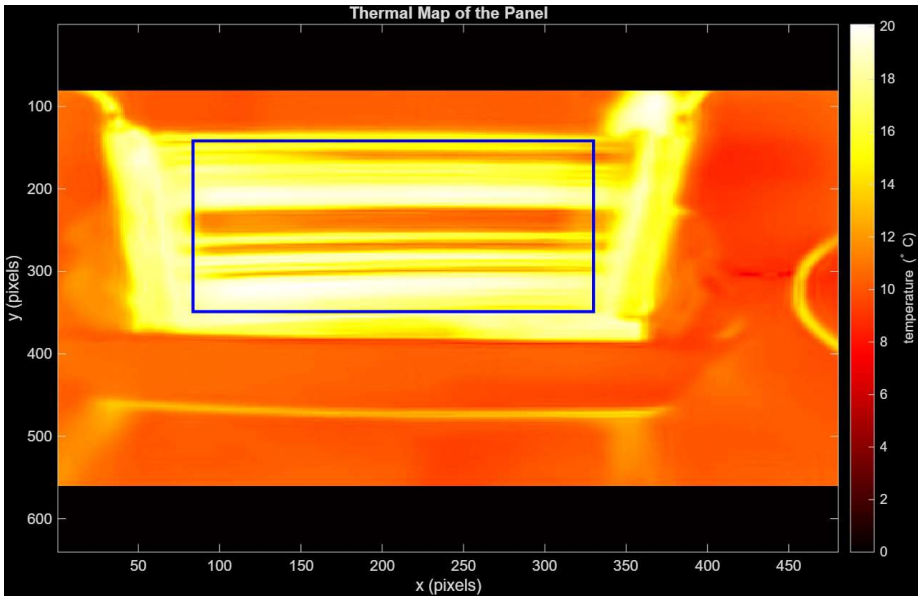

Figure C4 shows the Concept One Inlet to the Open Concpet Outlet and region of interest.

Copyright © 2026 by ASME

Appendix D

Figure D1: Pipe flow test illustrating the relationship between orifice depth and discharge velocity. Despite a partially filled manifold, the results clearly show that lower orifices experience higher internal pressure, resulting in the fastest jet streams.

Figure D2: Comparison of prototype manifolds used in discharge testing. The left images show the initial black manifolds where insufficient cleaning/deburring led to a negligible 1.8% flow improvement. The right images show the 3D-printed scaled models (blue and orange) with precise re-entrant orifices. These clean models demonstrated that under higher internal pressure at lower depths, discharge velocity improved by 26%.

Copyright © 2026 by ASME

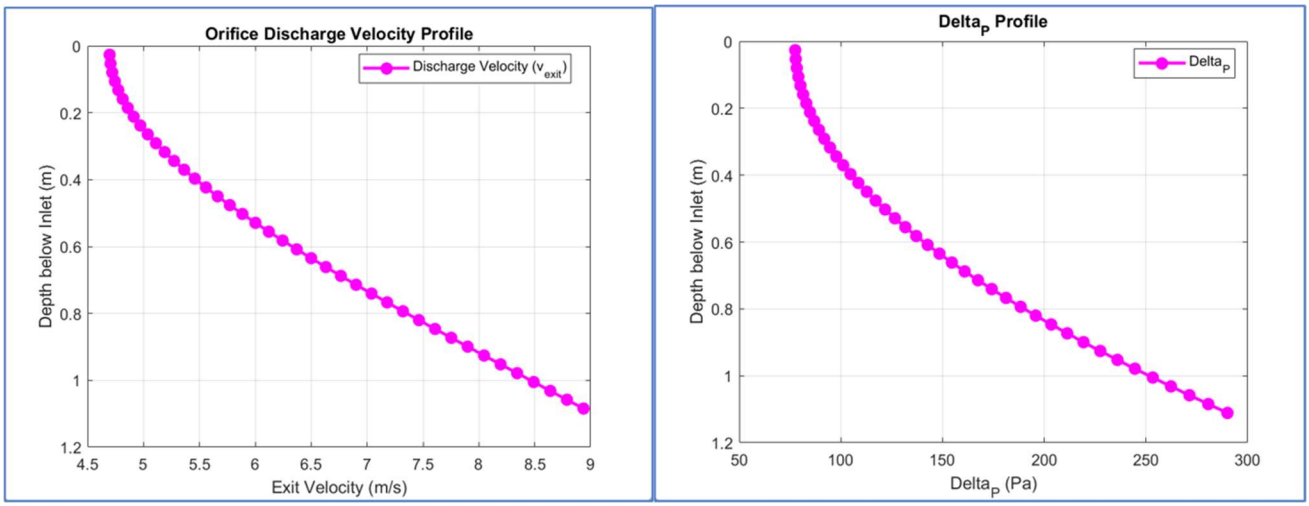

Figure D3: MATLAB simulation of the baseline manifold's hydraulic profile. The plots illustrate the non-linear increase in exit velocity and pressure differential (ΔP) as depth below the inlet increases. This theoretical model served as the foundation for the "choking" strategy, identifying the need to redistribute flow to the upper orifices to achieve uniformity.

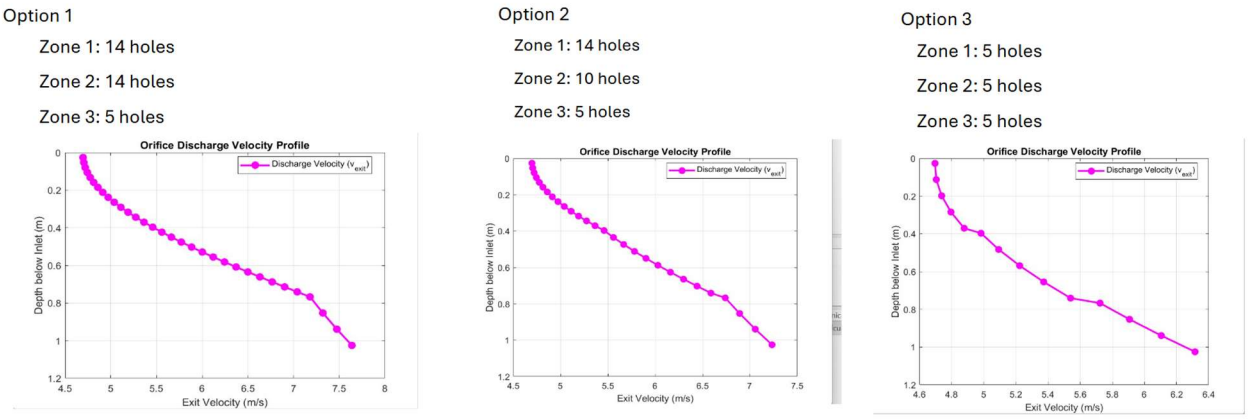

Figure D4: MATLAB iterations demonstrating the impact of orifice reduction on flow distribution. By reducing the number of orifices in the lower zones (Option 1 to Option 3), the discharge velocity curve becomes more vertical, indicating a significant reduction in velocity variation and a corresponding increase in flow uniformity across the manifold's length.

Table 13: Temperature Variation Across Panel Additional Testing -
These results remain inconclusive and require more testing because C1-B1 burst during the second phase of testing.

Designs	Mean [˚C]	Standard Deviation [˚C]	Max [˚C]	Min [˚C]	Coefficient of Variation
B1 – B1	19.41	3.94	27.21	10.15	0.2028
C1 – B1	21.93	5.45	21.14	11.29	0.2484
C1 – C1	21.61	3.68	28.4	10.80	0.1703
C1-Open	19.52	3.98	27.21	10.15	0.2038

These results remain inconclusive and require more testing because C1-B1 burst during the second phase of testing

Copyright © 2026 by ASME

Figure D5: Comparison of the full-scale MicroEra heat exchanger panel and the 50% scaled test models. The smaller manifolds shown in the foreground were utilized for physical flow testing and volume collection experiments to validate the "choking" strategy developed in MATLAB and CFD simulations.

Copyright © 2026 by ASME

Figure D6: Experimental test rig components. Top (left to right): Variac and ammeter for pump voltage regulation, water reservoir containing the submersible sump pump, and analog pressure gauge for inlet monitoring. Bottom: Assembled 50% scale manifold and panel model during flow testing.

Copyright © 2026 by ASME

APPENDIX E– MATLAB CODE

E.1

This code was used to determine the velocity profile of orifices as the depth descends.

pressureDropCalculator.m

```
clc; clear;
% Physical constants
rho = 1000;    % kg/m^3 % REPLACE THIS WITH ACTUAL FLUID PROPETIES
mu = 0.466*10^-3;    % Pa*s
epsilon = 1.5*10^-6;% m ; % surface roughness value. For a pipe, it's: ??
g = 9.81; % m/s^2

% Manifold geometry - can be edited after measurement
D_pipe = 1.3*0.0254; % m
A_pipe = (pi*D_pipe^2)/4; % m^2

%% Change number of orifices, denoted as "holes" in this section
Zone_spaceing = (43.75/39.37)/3; Z_offset = (43.75/39.37)/42;
a_holes = 14;
b_holed = 14;
c_holes = 4;

%%
A_distance = linspace(Z_offset,Zone_spaceing,a_holes);
B_distance = linspace(Zone_spaceing + Z_offset,Zone_spaceing*2,b_holed);
C_distance =  linspace(Zone_spaceing*2 + Z_offset,Zone_spaceing*3,c_holes);
L_segments = [A_distance, B_distance, C_distance]; % m from 0.8in orifice distance

% diameter of orifces
A = (0.121*0.0254) * ones(1,a_holes);
B = (0.121*0.0254) * ones(1,b_holed);
C = (0.121*0.0254) * ones(1,c_holes);
d_orifices = [A,B,C]; % can be dedited to be zones instead later. Employ array addition
h_depth_cumulative = L_segments; % Automatically calculate cumulative depth for external pressure P2
% This assumes the pipe inlet is at the water surface (Depth = 0)

% Initial State at Inlet (State 0)
H_pump_ft = 25.93; %25.93 ft from 2GPM flowrate
P_inlet = rho*g*(H_pump_ft*0.3048); % Pa, not outrageous like the 250 kpa we used before!!!!!
Q_current = 2 * 0.00378541 / 60; % m^3/s = L/s
V_inlet= Q_current/A_pipe; % m/s

% Z starts at 0 (surface) and goes negative as we go deeper
Length_mani = 43.75/39.37;% Lnegth of pipe
Z_current = 0;
P_current = P_inlet;
V_current = V_inlet;

num_holes = length(d_orifices);
fprintf('%-6s  %-10s  %-10s  %-10s  %-10s  %-10s  %-10s\n',  'Hole',  'Re',  'hf(m)',  'hm(o)',  'P_int(kPa)',
'P_ext(kPa)', 'V_exit');
results = zeros(num_holes, 4); % [Depth, Re, hf, V_exit]


for i = 1:num_holes
    % 1. Friction & Reynolds for the segment
    [Re, f] = calculateFrictionFactor(rho, V_current, D_pipe, mu, epsilon);
    hf = f * (L_segments(i) / D_pipe) * (V_current^2 / (2 * g));

    % 2. Calculate Internal State at Orifice i (State 1)
    Z_new = -1*(Z_current - h_depth_cumulative(i));
    P1 = P_current - rho * g * (Z_current - Z_new) - rho * g * hf;

    % 3. Calculate Orifice Exit (State 2)
    P2_external = rho * g * Z_new;% External static pressure
    P2_xxexternal(i) = P2_external/1000; %Storage
    P_differentials(i) = (P1 - P2_external)/1000; %Pa
    [hm, C] = calculateOrificeLoss(V_current, d_orifices(i), D_pipe);

    % What if I set v_exit to be
```


Copyright © 2026 by ASME

```
        A_o = pi *(d_orifices(i)/2)^2;
        ly = rho* (1 - (A_o/A_pipe));
        v_exit = C*sqrt((2*(P1 - P2_external))/ly);

        % Print Data Row
        fprintf('%-6d %-10.0f %-10.4f %-10.4f %-10.2f %-10.4f %-10.2f\n', i, Re, hf, hm, P1/1000, P2_external/1000,
v_exit);

        % 5. Update for Next Hole
        Q_exit = v_exit * ((pi * d_orifices(i)^2) / 4);
        Q_current = Q_current - Q_exit;

        V_current = Q_current / A_pipe;
        P_current = P1;
        results(i, :) = [h_depth_cumulative(i), Re, hf, v_exit];
    end


    % --- Plotting the Velocity Profile ---
    figure('Color', 'w');
    plot(results(1:end-1,4), results(1:end-1,1), 'mo-', 'LineWidth', 2, 'MarkerFaceColor', 'm');
    set(gca, 'YDir', 'reverse'); % Put Depth 0 at the top
    grid on;
    xlabel('Exit Velocity (m/s)');
    ylabel('Depth below Inlet (m)');
    title('Orifice Discharge Velocity Profile');
    legend('Discharge Velocity (v_{exit})', 'Location', 'best');

    % --- Plotting the delta_P Profile ---
    figure('Color', 'w');
    plot(P_differentials',results(:,1) , 'mo-', 'LineWidth', 2, 'MarkerFaceColor', 'm');
    set(gca, 'YDir', 'reverse'); % Put Depth 0 at the top
    grid on;
    xlabel('Delta_P (Pa)');
    ylabel('Depth below Inlet (m)');
    title('Delta_P Profile');
    legend('Delta_P', 'Location', 'best');

    % --- Required Functions ---
    function [Re, f] = calculateFrictionFactor(~, ~, D, ~, epsilon)
        Re = 1.6183e+05;% Indsutry standrad says water is turblent through pipe flow, so

        term1 = epsilon / (3.7 * D); %Kept so I didn't have to remake the function
        term2 = 5.74 / (Re^0.9);
        f = 0.25 / (log10(term1 + term2)^2);

    end

    function [h_m, C] = calculateOrificeLoss(v_pipe, d_orifice, D_pipe)
        g = 9.81;
        beta = d_orifice / D_pipe;
        C = (1 / (0.62 + 0.38 * beta^4) - 1)^2; %taking into account the burring/non-burring of the hole
        h_m = C * (v_pipe^2 / (2 * g));
    end
```

E.2

This code was used to calculate the pressure drop through up to five orifices.

Pressrue_Drop_Matrix_Solver.m

```
    clc; clear;

    K = 0.8; % Reentrant flow

    Cd = 0.5; % Confirm Cd
    g = 9.81; % Gravity m/s^2

    D_o = 0.121 * 0.0254; % meters
    A_o = pi*(D_o^2)/4; % Area of Orifie m^2
    % Distance between each orifice is 0.8 inches
    seg = linspace(1*0.0254,45*(0.8)*0.0254,44); % distacne between orifice [m]
```


Copyright © 2026 by ASME

```
    rho      = 1000; % density
    mu       = 0.466e-3; % dynami visosity
    epsilon  = 1.5e-6; % roughness of pipe
    D_m   = 1.3 * 0.0254; % diameter of diameter [m]
    A_m   = pi * D_m^2 / 4; % area of manifold [m]

    H_pump_ft  = 25.93; % Pump head ft
    P_pump_g   = rho * g * (H_pump_ft * 0.3048); % Pump Pressure [Pa]
    Pin  = P_pump_g; % Alloating inlet pressure to the system [Pa]
    Qin  = 2 * 0.00378541 / 60; % Volumetri Flow Rate in [m^3/s]
    % Length of Manifold is 45 inches
    L_total    = 45 / 39.37; % Length of manifold [m]

    %% Initialize Unkowns for Orifice Pressures and Flows
    Orifices = 4;
    for n = 1:Orifices
        Q_o{n} = sprintf('Q_o%d', n);
        P_o{n} = sprintf('P_o%d', n);
    end

    %% Initialize Unkowns for Junction Pressure and Flows

    Junctions = Orifices - 1;
    for n = 1:Junctions
        Q_j{n} = sprintf('Q_j%d', n);
        P_j{n} = sprintf('P_j%d', n);
    end

    %% Preallocate Space for equations
    Q_discharge = zeros(Orifices,1);
    Q_junction = zeros(Junctions,2);

    %% Symbolic Matrix
    S = sym([Q_o P_o Q_j P_j])

    %% Indexing
    Q_o_index   = 1:length([Q_o]);
    P_o_index   = length(Q_o)+1 : length([Q_o P_o]);
    Q_j_index = length([Q_o P_o])+1 : length([Q_o P_o Q_j]);
    P_j_index = length([Q_o P_o Q_j])+1 : length([Q_o P_o Q_j P_j]);

    %% Defining Variables
    vin = Qin/A_m;

    % velocities at orifices
    v_o = S(Q_o_index)/A_o;

    % velocities at junctions
    v_j = S(Q_j_index)/A_m;

    %% Energy Balance
    Energy_Balance = Qin == sum(S(Q_o_index));

    %% Junction Volumetric Flows
    for i = 1:length(Q_j_index)
        Junction_Flows(i) = S(Q_j_index(i)) == Qin - sum(S(Q_o_index(1:i)));
    end

    %% Flow from each Orifice
    Q_disharge = S(Q_o_index) == Cd*A_o*sqrt( (2/rho) * (Pin-S(P_o_index) ) );

    %% Juction Energy Balance

    % jx
    for i=1:length(Q_j_index)
        jx(i) = S(P_j_index(i))/(rho*g) + (1/2)*(v_j(i)^2)/g + seg(i) == S(P_o_index(i))/(rho*g) +
(1/2)*(v_o(i)^2)/g + seg(i) + K*(v_j(i)^2)/(2*g);
        jx_plus_1(i) = S(P_j_index(i))/(rho*g) + (1/2)*(v_j(i)^2)/g + seg(i) == S(P_o_index(i+1))/(rho*g) +
(1/2)*(v_o(i+1)^2)/g + seg(i+1) + K*(v_j(i)^2)/(2*g);
    end
```


Copyright © 2026 by ASME

```
    %% Putting all equations together into one matrix
    equations = [Energy_Balance, Junction_Flows, Q_disharge, jx, jx_plus_1];
    length(equations)
    unkowns = S;

    %% Solve
Y = vpasolve(equations,unkowns)
```

E.3

This code was used to determine the average temperature, standard deviation of temperature, max temperature, minimum temperature, and coefficient of temperature variation across each panel.

Thermal_Imaging_Code.m

```
    % thermal analysis code
    %% thermaCameraReader_v2, Boris, 4/8/2026
    clear, clc;
    [file_list, path_n] = uigetfile('.JPG','MultiSelect','on');
    if iscell(file_list) == 0
        file_list = {file_list};
    end
    for i = 1:length(file_list)
        filename = file_list{i};
        obj(i) = FlirMovieReader([path_n filename]);
        obj(i).unit = 'temperatureFactory';% Output in Celsuis
        [T, info] = read (obj(i));
        figure; imagesc(T); colormap hot
        hcb = colorbar; hcb.Label.String = 'temperature (^\circ C)';
        xlabel('x (pixels)'); ylabel('y (pixels)');
        title('Thermal Map of the Panel')
        pixelSize = 0.05; % (mm) replace with your value
        [x,y] = getpts
        left = x(1); % These need to be refresehd later
        bottom = y(2);
        right = x(2);
        top = y(1);
        hr = rectangle('position', [left bottom right-left top-bottom], ...
            'linewidth', 2, 'edgecolor', 'b');
        Trect = T(bottom:top,left:right); % thermal image within rectangle
        Ty = mean(Trect,2); % average over vertical direction
        y = (bottom:top)*pixelSize; % corresponding positions (mm)
        y = y-mean(y); % move origin to center of ribbon
        figure;
        plot(y,Ty)
        hold on
        ribbon1fit = fit(y(:),Ty(:),'poly2') % rename variables as appropriate
        plot(ribbon1fit)
        title('Spatial Temperature Variation - Y')
        xlabel('Position')
        ylabel('Temperature (C)')
    end

    mean = mean2(Trect)
    standard_deviation = std2(Trect)
    maximum = max(Trect,[],"all")
    minimum = min(Trect,[],"all")
    coeffiient_variation = standard_deviation/mean
```


Copyright © 2026 by ASME